

北海道大学
工学部研究報告

第 162 号

平成 5 年 1 月

金属工学科創立50周年記念号

北海道大学工学部



71.22
10.0

北海道大学
工学部研究報告

第162号

平成 5 年 1 月

金属工学科創立50周年記念号

目次

論文及び報告

〈材料物理化学〉

1. In situ Infrared Reflection Absorption Spectroscopy at an Electrode-Electrolyte Interface
in the Fingerprint Wave-Number Region Takeshi SASAKI and Tatsuo ISHIKAWA 1
2. 石炭液化油オイル成分の脱水素反応によるヒドロ芳香族構造に関する研究
.....横山 晋・金子雅仁・佐藤正昭・真田雄三 9
3. In-situ FT-IR 法を用いた石炭の乾燥に関する研究
.....熊谷治夫・Bruce A. Grigor・Russell F. Howe 21
4. Evaluation Methods of Coking Coal for Coke Manufacturing
—Hydrogen and Electron Transfer Abilities of Coal—
..... Y. SANADA, M. SASAKI and K. NAKAMURA 29
5. コークスガス化反応における水性ガス反応の種類 柏谷悦章・石井邦宜 37
6. 銅管の微細局部腐食メカニズムについて 能登谷武紀 45

〈材料物性〉

7. First-principles calculation of Diffuse Intensity Spectrum of Binary Alloys
..... Tetsuo MOHRI 55
8. Theoretical Study on the Phase Stability of Au-Pd System
..... Satoshi TAKIZAWA 63
9. Anisotropic Cyclotron Effective Mass and Local Fermi Surface Shape of lead
..... S. WATANABE and H. TAKAHASHI 73
10. Fe-Cr-Ni モデル合金における電子線照射挙動の損傷速度依存性
..... 高橋平七郎・橋本直幸 81
11. 低炭素焼入マルテンサイト鋼の再結晶に及ぼす固溶型 MnS の影響
..... 田海啓司・伊藤洋一・成田敏夫 91

〈材料組織〉

12. Martensitic Transformation of Antiferro-magnetic Fe Particles Embedded in a Cu
Matrix in a Magnetic Field Yoshimi WATANABE, Masaharu KATO and A. SATO 99
13. 水素・重水素イオン注入によるAlの組織変化 木下博嗣・高橋平七郎 109

14. TEM Observation of Magnetite Reduction With Implanted HydrogenK. ISHII, M. KATSUMI, Y. TAMURA, Y. KASHIWAYA and S. SATOH	117
15. 多結晶 Si/単結晶 Si 界面における自然酸化膜の球状化現象大賀 惣明・木村 道哉・高橋平七郎・木村 幸治・熊丸 邦明	127
16. 安定化ジルコニアの活性金属ろうとの反応による変色挙動三枝 利紀・成田 敏夫	137
17. MoSi ₂ 基材料の耐酸化性黒川 一 哉・W. L. Worrell	149
<材料加工>	
18. Al 基三元合金の凝固パスの解析大笹 憲一・大宮 光裕・工藤 昌行・大参 達也	163
19. 複合鑄込み法による過共晶 Al-Si 系合金の初晶微細化機構大参 達也・田中 康博・工藤 昌行・大笹 憲一	173
20. 拡散対による Fe-C 系の包晶反応速度の測定松浦 清隆・伊藤 洋一・成田 敏夫	185
21. 酸化物フラックスによる炭素鋼の大過冷却工藤 昌行・田中 順一・奥山浩二郎・大笹 憲一	191
22. 亜共晶 Mg-Li 合金の変形集合組織に及ぼす圧延温度の影響伊藤 洋一・松浦 清隆・田海 啓司・米澤 襄・成田 敏夫	203
23. Ni-NiO 系, Ni-Si ₃ N ₄ 系, Ni-AlN 系並びに Al-AlN 系の傾斜機能材料新谷 光二	213
<プロセッシング>	
24. 微粒子の気系流動化による定量供給千葉 忠俊	219
25. 塩化白金酸水溶液の水素還元による白金微粉末の製造に関する基礎的研究木内 弘道・坂下 浩朗・安田 拓夫	231
26. 連続式オートクレーブを用いた不均化反応による銅微粉末製造法の研究佐々木 仁・永井 忠雄	241
27. Development of Graphite Cathodes for an Aluminum-Chlorine Fuel Cell in High Temperature Chloride MeltsTatsuo ISHIKAWA, Takeshi SASAKI, and Shoichi KONDA	255
28. 塩化アルミニウム含有塩化物溶融塩におけるアルミニウムの電析形態ならびにその評価法近田 昭一・松田 隆明・石川 達雄	265
29. Effects of Porosity and Slag Former Amount on Rate of Heating-up Reduction of Self-fluxed Pellet.Jalil Vahdati khaki, Yoshiaki KASHIWAYA and Kuniyoshi ISHII	273

BULLETIN
OF THE
FACULTY OF ENGINEERING
HOKKAIDO UNIVERSITY

No. 162

January, 1993

IN COMMEMORATION OF THE FIFTY ANNIVERSARY OF
DEPARTMENT OF METALLURGICAL ENGINEERING

NOTICE

Papers and Reports	Author	Page
Physical Chemistry of Materials		
1. In situ Infrared Reflection Absorption Spectroscopy at an Electrode-Electrolyte Interface in the Fingerprint Wave-Number Region	Takeshi SASAKI and Tatsuo ISHIKAWA	1
2. Hydroaromatic Ring Structure of Coal Hydrogenation oil by Means of Dehydrogenation and HPLC-GC-LV MS	Susumu YOKOYAMA, Masahito KANEKO, Masaaki SATOU and Yuzo SANADA	9
3. In-situ FT-IR Spectroscopic Studies of Coal Drying	Haruo KUMAGAI, Bruce A. Grigor and Russell F. Howe	21
4. Evaluation Methods of Coking Coal for Coke Manufacturing —Hydrogen and Electron Transfer Abilities of Coal—	Y. SANADA, M. SASAKI and K. NAKAMURA	29
5. Water gas reaction in coke gasification by H ₂ O.	Yoshiaki KASHIWAYA and Kuniyoshi ISHII	37
6. Mechanisms of Localized Corrosion in Copper Tubes	Takenori NOTOYA	45
Property of Materials		
7. First-principles calculation of Diffuse Intensity Spectrum of Binary Alloys	Tetsuo MOHRI	55
8. Theoretical Study on the Phase Stability of Au—Pd System	Satoshi TAKIZAWA	63
9. Anisotropic Cyclotron Effective Mass and Local Fermi Surface Shape of lead	S. WATANABE and H. TAKAHASHI	73
10. Damage Rate Dependence of Electron-Irradiation Behaviors in Fe-Cr-Ni Model Alloy	Heishichiro TAKAHASHI and Naoyuki HASHIMOTO	81
11. The effect of Precipitated MnS on Recrystallization in Low Carbon Martensite Steel	Hiroshi TAUMI, Yoichi ITO and Toshio NARITA	91
Structure of Materials		
12. Martensitic Transformation of Antiferro-magnetic Fe Particles Embedded in a Cu Matrix in a Magnetic Field ...	Yoshimi WATANABE, Masaharu KATO and A. SATO	99
13. Microstructural change of Al on Hydrogen or Deutrium ion implantation	Hiroshi KINOSHITA and Heishichiro TAKAHASHI	109

14. TEM OBSERVATION OF MAGNETITE REDUCTION WITH IMPLANTED HYDROGEN	K. ISHII, M. KATSUMI, Y. TAMURA, Y. KASHIWAYA, and S. SATOH	117
15. Balling-up Phenomena of Native Oxide Film on Poly-Si/Single-crystal Si InterfaceSomei OHNOKI, Michiya KIMURA, Heishichiro TAKAHASHI, Koji KIMURA and Kuniaki KUMAMARI	127
16. Coloring Behavior of Stabilized Zirconia in the Reaction with Active Metal SolderToshiki MITSUEDA and Toshio NARITA	137
17. High temperatur oxidation of MoSi ₂ based materialsKazuya KUROKAWA, W. L. WORRELL	149
Forming of Materials		
18. Analysis of Solidification Path of Aluminum Base Ternary AlloyKenichi OHSASA, Mitsuhiro OHMIYA, Masayuki KUDOH and Tatsuya OHMI	163
19. Refining Mechanism of Primary Crystals in Hypereutectic Al-Si Alloy Ingots by the Duplex Casting ProcessTatsuya OHMI, Yasuhiro TANAKA, Masayuki KUDOH and Ken-ichi OHSASA	173
20. Measurement of Growth Rate of Austenitic Phase during Peritectic Reaction in an Fe-C SystemKiyotaka MATSUURA, Youichi ITOH and Toshio NARITA	185
21. Large Undercooling due to Oxide Flux in Plain Carbon SteelMasayuki KUDOH, Jun-ichi TANAKA, Kohjiroh OKUYAMA and Ken-ichi OHSASA	191
22. Effect of Rolling Temperatures on the Deformation Texture of Hypo-eutectic Mg-Li AlloyYouichi ITOH, Kiyotaka MATSUURA, Hiroshi TAUMI, Noboru YONEZAWA and Toshio NARITA	203
23. Functionally Gradient Materials of Ni-NiO, Ni-Si ₃ N ₄ , Ni-AlN and Al-AlN Systems.Koji ATARASHIYA	213
Materials Processing		
24. A Solid Feeder of Fluidised Agglomerates of Fine ParticlesTadatoshi CHIDA	219
25. A Fundamental Study of the Production of Fine Platinum Powder by Hydrogen Reduction of a Chloro-Platinum Acid Aqueous SolutionHiromichi KIUCHI, Hiroaki SAKASITA and Takuo YASUDA	231
26. Production of Fine Copper Powder by Disproportionation Reaction of Cuprous Sulfate Solution using a Continuous Type AutoclaveHitoshi SASAKI and Tadao NAGAI	241
27. Development of Graphite Cathodes for an Aluminum-Chlorine Fuel Cell in High Temperature Chloride MeltsTatsuo ISHIKAWA, Takeshi SASAKI, and Shoichi KONDA	255
28. Electrodeposition Forms of Solid Aluminum and Estimation of their Smoothness in Low Temperature Chloride Melts containing AlCl ₃Shoichi KONDA, Takaaki MATSUDA and Tatsuo ISHIKAWA	265
29. Effects of Porosity and Slag Former Amount on Rate of Heating-up Reduction of Self-fluxed Pellet.Jalil Vahdati khaki, Yoshiaki KASHIWAYA and Kuniyoshi ISHII	273

In situ Infrared Reflection Absorption Spectroscopy at an Electrode-Electrolyte Interface in the Fingerprint Wave-Number Region

Takeshi SASAKI and Tatsuo ISHIKAWA

(Received September 18, 1992)

Abstract

In order to extend the wave number to the fingerprint region in *in situ* infrared spectroscopy for an electrode system, new techniques were developed. First, a new test cell equipped with a micrometer attached to the test electrode and an O-ring for setting an optical window was made of Kel-F. The cell prepared a thin electrolyte layer imposed between the window and the test electrode, as a stable state during experiments. Next, a new manipulation system for treating the piston attached to the test electrode was devised. This made it possible to manipulate the piston without any interference with the purging effect of N₂ gas. With these new techniques we succeeded in the acquisition of significant signals of monolayer-adsorbed aromatic thiols in the fingerprint region.

The spectra showed that both 2,5-dihydroxythiophenol (DTH) and p-mercaptophenol (MP) adsorbed on the surface of gold with the molecular plane nearly perpendicular to the electrode surface and that the oxidation states changed with the potential changes.

1. Introduction

Infrared spectroscopy of molecules adsorbed on a metal surface provides fundamental information about the modification of metal surfaces and electrocatalytic reactions. Since the Southampton group succeeded in the application of infrared spectroscopy to an electrode system, by the *in situ* outer reflection absorption technique^{1,2)}, this method has become one of the most powerful techniques to elucidate electrode kinetics and to develop modified electrodes, and many groups around the world have applied the technique to electrode systems. Even though great efforts have been made to improve the technique, the wave number region where significant peaks can be obtained is still limited and vibration modes are also limited to very strong signals such as the C-O stretching of carbon monoxide, the C=O stretching of aldehyde, the C≡N stretching of cyanide and so on.

We developed new techniques in order to extend the applicable wave number to the fingerprint region^{3,4)}, where the signals contain much information about organic molecules adsorbed on electrode surfaces. The objective of this study is to report these new techniques and to demonstrate some results for 2, 5-dihydroxythiophenol (DTH) and p-mercaptophenol

(MP) adsorbed on polycrystalline gold surfaces.

2. Experimental

Application of *in situ* infrared spectroscopy to an electrode system involves special difficulties, since the signals from monolayer-adsorbed molecules are very small and water strongly absorbs infrared light. To overcome these difficulties, the electrolyte layer between a working electrode and an optical window should be made as thin as possible, only a few microns thick, and should be stable during a series of experiments. Therefore it is essential to set the working electrode strictly parallel to the optical window.

The test cell prepared for both electrochemical and spectroscopic experiments and the reservoir for solutions are schematically presented in Fig. 1.

The cell is composed of a body block and a piston made of Kel-F rods and an optical window made of a 65° calcium fluoride dove prism connected with the body by using an O-ring. The window plane can be set strictly parallel to the electrode surface by setting the three screws of the window holder (not shown in the figure) with the guidance of interference rings formed in the thin electrolyte layer. The working electrode is pushed against the window or withdrawn from it by manipulating the micrometer, which fixes the thickness of the electrolyte film stably. This was accomplished by using the O-ring and the micrometer. Usually we carried out both spectroscopic and electrochemical experiments while pushing the electrode surface against the window.

The reservoir, made of pyrex glass, has a compartment for a reference electrode, and is electrically connected with the test cell through an electrolyte in a thin teflon tube.

The test electrode was prepared by molding a gold plate (99.99 %, Johnson Matthey Co.) in Kel-F powder at 300 °C under high pressure⁵⁾ and working it with a lathe. The counter electrode was a platinum wire, and a saturated calomel electrode or a silver-silver chloride electrode was employed as a reference electrode. The potential is described by referring to NHE in this work.

Solutions were made with Ultrex grade HClO_4 (Baker) and triply distilled water and were thoroughly deaerated with high-purity N_2 gas. In this study, 0.1 M HClO_4 was used throughout all experiments as a base electrolyte. DHT was synthesized by the method of Alcalay⁶⁾, and later extracted and recrystallized in ether. MP of reagent grade was used as received (Wako Pure Chemical Ind. Ltd.).

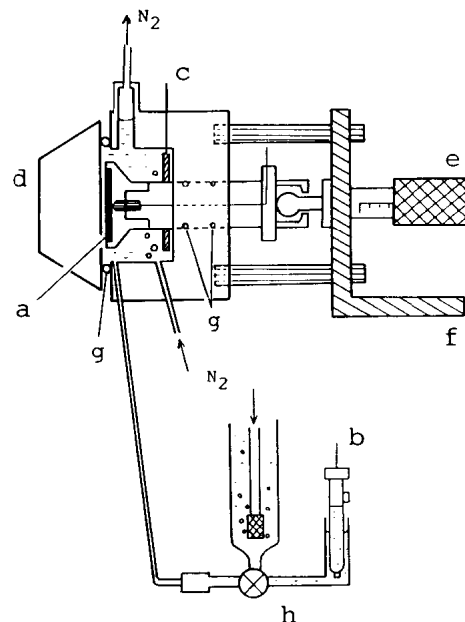


Fig. 1 Schematic diagram of a spectroelectrochemical cell and a reservoir. a: test electrode (Au plate), b: reference electrode, c: counter electrode (Pt wire), d: CaF_2 window, e: micrometer, f: cell holder, g: o-ring, h: reservoir.

The optical arrangement in the sample room of the Fourier transform infrared spectrometer (IR/98, IBM Instruments, Inc. or FT/IR 8000, Japan Spectroscopic Co., Ltd.) and the measurement apparatus are shown in Fig. 2.

A p-light selected by a polarizer radiated to the electrode with an incident angle of 65° and went into a liquid-nitrogen-cooled HgCdTe detector. During the measurements, the piston was manipulated from outside the sample room, which was purged continuously with N_2 gas throughout all experiments. This manipulation did not interfere with any purging effect of the sample room, and it led to success in the acquisition of spectra in the fingerprint region. This is the other main point of this technique, because atmospheric water also hides most of the significant peaks in this wave-number region.

The test electrode was polished to an mirror finish with a series of alumina powders of successively smaller size down to $0.3\ \mu\text{m}$. After rinsing with alcohol and distilled water, the electrode was cleaned by ultrasonic waves for a short time. Before every experiment the electrode was cleaned by cycling potential between hydrogen evolution and oxygen evolution in $0.1\ \text{M}\ \text{HClO}_4$ until the characteristic features of clean surfaces appeared.

After cleaning the electrode, the electrolyte was replaced with a solution containing $10\ \text{mM}$ organic materials several times, finally keeping the solution in the cell for 10 minutes to place organic materials in contact with the electrode. Next, the solution was replaced with neat perchloric acid several times to remove the organic materials remaining in the electrolyte without adsorption to the electrode. Then, the electrode was pushed against the window and the spectroscopic or electrochemical experiments were carried out.

In the optical experiments, the spectra were acquired and plotted by SNIFTIRS (subtracted normalized interfacial Fourier transform infrared spectroscopy). By this technique a reference spectrum is acquired at a special value as a reference potential and sample spectra are measured at the desired sample potentials. The reflectivity difference between the sample and the reference is divided by the reference reflectivity for normalization, which can make a small signal originating from a monolayer substance very clear. In the spectra plotted by this formula, positive-going peaks come from the sample and negative-going peaks come from reference states.

The interferograms between 1000 and 2000 were collected and co-added at each potential to improve the S/N ratio.

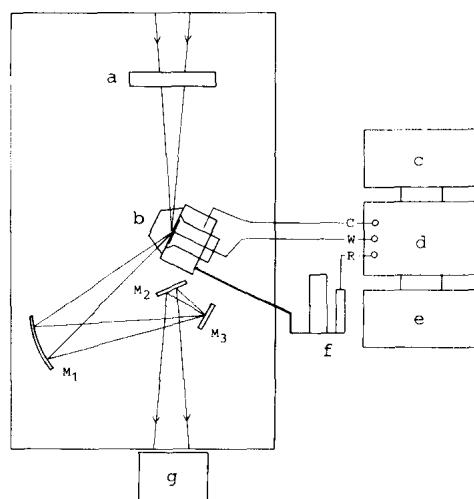


Fig. 2 Optical arrangement and measurement apparatus. a: polarizer, b: spectroelectrochemical cell, c: function generator, d: potentiostat, e: recorder, f: reservoir, g: HgCdTe detector, M_1 : spherical mirror, M_2 , M_3 : plane mirror.

3. Results and discussion

A cyclic voltammogram of DHT and that of MP are shown in Fig. 3 and Fig. 4, respectively. As shown in the figures, there is one peak on the oxidation wave and one on the reduction wave for both compounds. Neither the positions nor the heights of these peaks change with repetitions of the cycling potential and replacements of the electrolyte.

Since DHT adsorbs to Au electrodes forming a mercaptide bond between S and Au⁷⁾, it is concluded from Fig. 3 that DHT adsorbs irreversibly on the surface of gold and the redox reaction occurs reversibly as it adsorbs; the reduced state is the hydroquinone-type and the oxidized state is the quinone-type.

The quantities of electricity shown by the peak areas in Fig. 3 are nearly the same and equal to ca. 1.4×10^{-4} coulomb/cm² (7.3×10^{-10} mol/cm²). According to Soriaga and co-workers⁸⁾, this value corresponds to the full monolayer coverage of DHT when the roughness factor of the electrode is 1.3, which is a reasonable value for the mirror-finished surface of gold.

The quantity of electricity for MP is, on the other hand, 3.7×10^{-5} coulomb/cm². The coverage is calculated to be nearly 0.5 by assuming that the occupation area of MP is nearly equal to DHT, since we do not have any data about the occupation area of MP.

A series of spectra were measured by SNIFTIRS in the DHT system and the results are presented in Fig. 5. As indicated in Fig. 5, first, a number of positive- and negative-going peaks could be clearly identified at the potential of +0.84 V, after which they disappeared at +0.34 V. This is consistent with the cycling voltammogram in Fig. 3, that is, the materials were in the oxidized state at +0.84 V, and at +0.34 V, they returned to the reduced state and the peaks disappeared, since the reference spectrum is for the reduced state. The rather strong signals observed suggest that the various normal vibration modes have dynamic dipole moments with components along a direction perpendicular to the electrode surface and that the modes are capable of interacting with the electric field vector for light polarized parallel to the plane of incidence. This provides evidence that the adsorbate, both in the

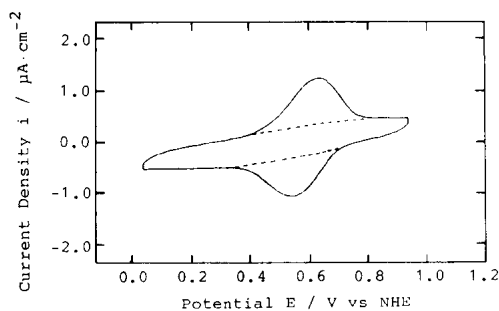


Fig. 3 Cyclic voltammogram of monolayer-adsorbed DHT on a Au electrode (surface area is 1.7 cm²). Scan rate is 1 mV/sec. The dashed lines represent the capacitive contribution of the interface.

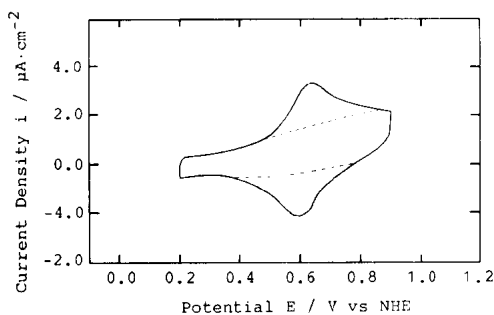


Fig. 4 Cyclic voltammogram of monolayer-adsorbed MP on a Au electrode (surface area is 1.6 cm²). Scan rate is 10 mV/sec. The dashed lines represent the capacitive contribution of the interface.

reduced and oxidized forms, is coordinated to the surface with the molecular plane perpendicular, rather than parallel to, the substrate.

Considerable insight into the nature of these spectrum features could be obtained from FTIR reflection absorption experiments involving a thicker layer of a DHT solution interposed between the window and the electrode surface. Figure 6 shows the spectrum obtained with unpolarized light for a solution of 50 mM DHT in 0.1 M HClO_4 that was electrolyzed for 150 min at a potential of 0.5 V. This spectrum displays a number of prominent features: (i) a negative-going band at 1211 cm^{-1} , which is characteristic of C-O stretching arising from the hydroquinone form of the compound,⁹⁾ (ii) two positive-going bands at 1277 and 1319 cm^{-1} associated with C-C stretching modes,¹⁰⁾ (iii) two negative-going bands at 1501 and 1454 cm^{-1} , which may be assigned to C=C skeletal deformation of the benzene ring.^{10, 11)} These observations are consistent with a hydroquinone-quinone-type redox process.

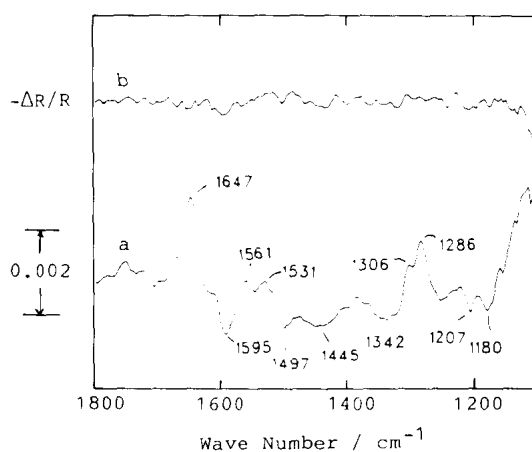


Fig. 5 Normalized difference IRRAS spectra of DHT adsorbed on a Au electrode. The spectrum obtained at $+0.34\text{ V}$ was used as a reference. The curve a at $+0.84\text{ V}$ was recorded first and next the curve b at $+0.34\text{ V}$ was recorded.

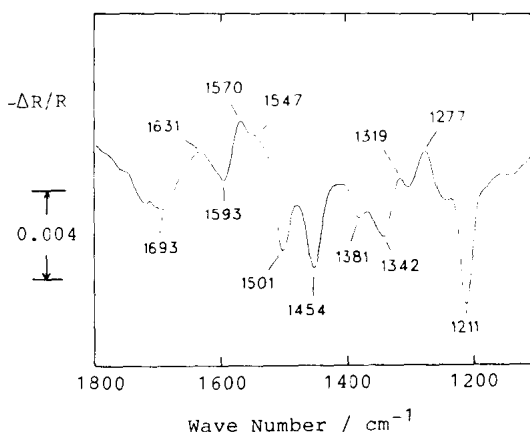


Fig. 6 Normalized difference IRRAS spectrum of a solution of 50 mM DHT in 0.1 M HClO_4 electrolyzed for 150 min at a potential of $+0.74\text{ V}$ with the spectrum obtained at $+0.34\text{ V}$ as a reference.

On the other hand, the increase in intensity of the difference spectrum in the wave-number region below 1150 cm^{-1} is due to the existence of a peak from perchlorate ions at 1107 cm^{-1} .¹²⁾ The perchlorate ions diffuse into the thin electrolyte layer to hold the electric neutrality in the course of electrolysis.¹³⁾

Although the similarities between the spectra obtained in solution and on the surface *in situ* are marked, there are some differences that deserve further attention. These include the much-decreased relative intensity of the peak at about 1211 cm^{-1} for the surface-bound species compared with those at 1319 and 1277 cm^{-1} and the slight shifts in energies. In fact, a careful inspection of Fig. 5 affords some evidence for a splitting of the 1211 cm^{-1} peak into two bands. This effect may be related to the inequivalency of the two C-O bonds, which may become particularly pronounced upon adsorption of DHT to the surface.

The same experimental procedure was carried out in the MP system as in the DHT system, and the spectra of MP adsorbed and in electrolyte are shown in Fig. 7 and Fig. 8.

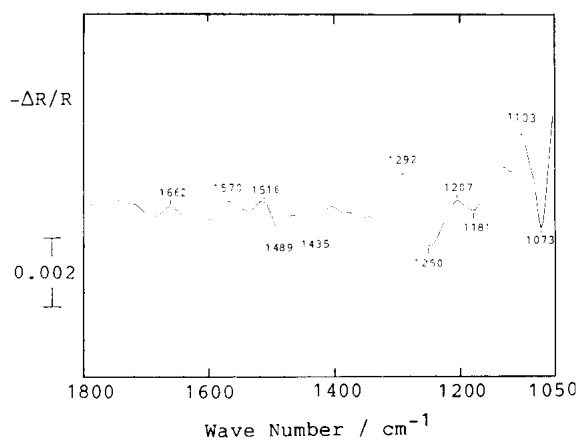


Fig. 7 Normalized difference IRRAS spectrum of MP adsorbed on a Au electrode. The spectrum was measured at $+0.9\text{ V}$ with the spectrum obtained $+0.2\text{ V}$ as a reference.

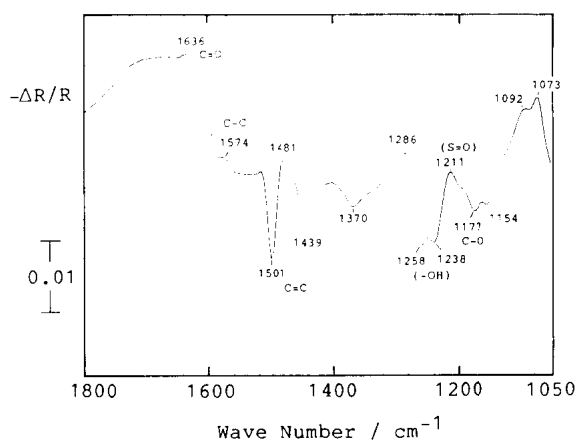


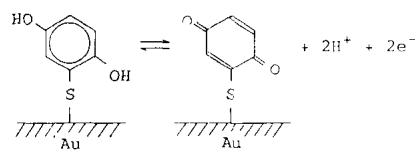
Fig. 8 Normalized difference IRRAS spectrum of a solution of 20 mM MP in 0.1 M HClO_4 electrolyzed for 15 min at a potential of $+0.9\text{ V}$ with the spectrum obtained at $+0.2\text{ V}$ as a reference.

The vibration modes were investigated as in the case of DHT and the assigned modes are presented in Fig. 8. In this figure, the positive-going peak of 1636 cm^{-1} associated with C=O stretching vibration is apparently very small due to overlapping of the deformation vibration peak of water. Two large negative-going bands of 1258 and 1238 cm^{-1} may be assigned to C-O stretching.¹⁴⁾ It was very difficult to assign a C=S stretching mode in the figure, since the intensity was usually low and it easily changed position depending on the substituents.¹⁴⁾ But the band of 1211 cm^{-1} may be associated with the C=S stretching vibration. The band from the C-S bond was positioned at lower than 1000 cm^{-1} and we could not detect the band due to the usage of the CaF_2 window. Although no modes related to sulfur could be clearly assigned in this experiment, MP also changed the oxidation state between the hydroquinone type and the quinone type with potential change as DHT did, since C=O and C-O modes were observed.

By comparing Fig. 7 with Fig. 8, the spectra of MP adsorbed on the electrode surface were seen to be similar to those in solutions such as DHT, the peak shifts were very small, but some peaks changed their relative heights. Further investigations of these changes remain to be carried out.

The bands associated with the skeletal deformation of the benzene ring were observed in the spectra shown in Fig. 5 and Fig. 7. This concludes that both DHT and MP adsorb to the gold surface with the molecular plane nearly perpendicular to the electrode surface. The schematic diagrams of the adsorbed DHT and MP with their redox changes are presented in Fig. 9.

2,5-Dihydroxythiophenol



p-Mercaptophenol

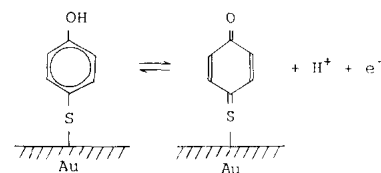


Fig. 9 Schematic diagram of the oxidation and reduction of the adsorbed DHT and MP.

4. Conclusions

As shown in this report, we succeeded in the acquisition of significant signals of monolayer-adsorbed aromatic thiols in the fingerprint region by using a new cell and arrangement in the sample room. The spectra show that both DHT and MP adsorb to the surface of gold with the molecular plane nearly perpendicular to the electrode surface and change the oxidation states with the potential changes.

Acknowledgment

The authors greatly appreciate that a part of this work was supported by a grant-in aid of Asahi Glass Foundation.

References

- 1) Bewick, A. and Kunimatsu, K., *Surface Science*, **101** (1980) 131.
- 2) Bewick, A., Kunimatsu, K. and Pons, B. S., *Electrochim. Acta*, **25** (1980) 465.
- 3) Sasaki, T., Bae, I. T., Scherson, D. A., Bravo, B. G. and Soriaga, M. P., *Langmuir*, **6** (1990) 1234.
- 4) Sasaki, T. and Ishikawa, T., *Hyomen Gijyutu*, **43** (1992) 457.
- 5) Anderson, J. E., Tallman, D. E., Chesney, D. J. and Anderson, J. L., *Anal. Chem.*, **50** (1978) 1051.
- 6) Alcalay, W., *Helv. Chim. Acta*, **30** (1947) 578.
- 7) Bravo, B. G., Mebrahtu, T., Soriaga, M. P., Zapien, D. C., Hubbard, A. T. and Stickney, J. L., *Langmuir*, **3** (1987) 595.
- 8) Bravo, B. G., Michelhaugh, S. L. and Soriaga, M. P., *J. Electroanal. Chem.*, **241** (1988) 199.
- 9) Silverstein, R. M., Bassler, G. C. and Morrill, T. C., *Spectrometric Identification of Organic Compounds*, 4th ed., p108, (John Wiley & Sons, 1981).
- 10) Davies, M. and Prichard, F. E., *Trans. Faraday Soc.*, **59** (1963) 1248.
- 11) Prichard, F. E., *Spectrochim. Acta*, **20** (1964) 1283.
- 12) Nakamoto, K., *Infrared and Raman Spectra of Inorganic and Coordination Compounds*, p130, (Wiley, 1986).
- 13) Bae, I. T., Xing, X., Yeager, E. B. and Scherson, D. A. *Anal. Chem.*, **61** (1989) 1164.
- 14) Bellamy, L. J., *The Infrared Spectra of Complex Molecules*, 3rd ed., p. 122, p. 394 (Chapman and Hall, 1975).

石炭液化油オイル成分の脱水素反応による ヒドロ芳香族構造に関する研究

横山 晋 金子 雅仁
佐藤 正昭 真田 雄三

(平成4年9月18日受理)

Hydroaromatic Ring Structure of Coal Hydrogenation Oil by Means of Dehydrogenation and HPLC-GC-LV MS

Susumu YOKOYAMA, Masahito KANEKO,
Masaaki SATOU and Yuzo SANADA

(Received September 18, 1992)

Abstract

Coal hydrogenation liquid consists of various aromatic ring and naphthenic ring structure condensed to their aromatic ring (hydroaromatic ring) designated as compound type. The chemical structures of these compound types were investigated by HPLC-GC-LV MS to estimate the number of aromatic and naphthenic ring and a representation method for their structural results was proposed. However, the absolute chemical structure of hydroaromatic species can not be elucidated because mass analysis is difficult to distinguish among isomers which have identical molecular weight but different ring structures.

In this study, dehydrogenation reaction were performed on various compound classes separated by amine column HPLC for SRC-II oil and the hydroaromatic compounds were converted to the corresponding polyaromatic compounds which were analysed by means of GC-LV MS. Species of hydroaromatic ring types consisting of five and six member naphthene ring were clarified.

1. ま え が き

石炭の高圧水素化分解反応による生成油オイル分(n-ヘキサン可溶分)について、これまで色々な構造解析法が開発されて、構成成分の化学構造が究明されてきた。これより、石炭水添生成油は芳香族化合物が主要成分として構成されており、種々の芳香環にアルキル基および含酸素官能基の多様な置換構造のために極めて複雑な混合成分からなることが分かった^{1,2)}。一方、石炭の化学構造について、1959年、Lahiri ら³⁾は石炭を硫黄と共に加熱すると、石炭構造のヒドロ芳香族の

ナフテン環部分で脱水素されて硫化水素が発生することを見だし、ナフテン環構造の存在を初めて示唆した。石炭の熱分解反応において、このナフテン環の水素が生成ラジカルへ付加して安定化させるのに重要な働きを担っている事が分かった。Curtis ら⁴⁾は石炭のこの水素供与能を、ナフテン環の脱水素反応による生成水素量から評価している。最近、同様な評価を行うために、アントラセンを水素授与体に用いた簡便法が報告されている⁵⁾。

石炭水添生成油のオイル分にヒドロ芳香族環構造を含む事は、上述の石炭構造からも示唆されるものであり、且つ水素化反応による芳香族環の飽和も平行して起きているものと考えられる。石炭水添液化油のナフテン環構造について、大内ら⁶⁾は元素分析および¹H-NMR スペクトルの結果から全環数 R と芳香環数 Ra を求め、これよりナフテン環数 Rn を $Rn = R - Ra$ によって間接的に求めた。この結果、構造単位の構成にナフテン環が重要な部分を占めることを示した。

石炭の水素化分解反応においても、溶剤の水素供与能は石炭高分子の分解による低分子ラジカルの安定化のために重要であり、溶剤の効果を表す大切な指標である。これはヒドロ芳香族のナフテン環水素が脱水素されて同様な働きをする。この溶剤効果を表す水素供与能として、¹³C-⁷⁾、¹H-NMR スペクトル^{8, 9)}によってヒドロ芳香族環のナフテン環炭素、水素を測定して、評価する方法が提出されている。これはナフテン環構造の炭素数、水素数を平均的に解析するものである。これに対して、HPLC-LV MS 法は液化油を飽和炭化水素、1, 2, 3 環、多環芳香族、極性化合物の各フラクション（化合物クラスと称す）毎に分別し、この分子イオンの質量 (MS) スペクトルから芳香環-ナフテン環（化合物タイプと称する）数を解析するものである¹⁰⁾。これより、芳香環及びヒドロ芳香環の環分布及び化合物タイプ同族体の分子量分布として、より詳細な化学構造を評価する事ができる。

HPLC-LV MS 法によって、石炭水添液化オイル分の化合物タイプ及びこの同族体の構造解析を行った結果、ヒドロ芳香族構造が重要な構造要素である事が分かった¹¹⁾。しかし、この解析によって求められる知見は芳香環-ナフテン環の各環数であり、環構造や 5 員環、6 員環ナフテンの識別などの異性体についての知見は殆ど与えない。そこで本研究では脱水素反応と HPLC-LV MS 解析法を組み合わせる事によって、液化油のヒドロ芳香族環構造の解明を試みた。

2. 実 験

2.1 試料

The Pittsburg & Midway Coal Mining Co. における、Solvent Refined Coal（溶剤精製炭：SRC-II）パイロットプラントで製造された SRC-II 生成油の重質留分 (bp. 288-454°C) である。元素分析値；C：90.0, H：7.8, N：1.1, S：0.5, O：0.5（差）(wt. %)。

2.2 HPLC-GC-LV MS 法による構造解析

山村化学社製 NH₂ カラム (I. D. 20mm) を装着した HPLC によって、芳香族環数毎に Fr-P（飽和炭化水素）、M（1 環芳香族類）、D1（ナフタレン型 2 環芳香族類）、D2（ビフェニール型 2 環芳香族類）、T1（3 環芳香族類）、T2（多環芳香族類）及び PP（極性化合物）の各化合物クラスに分別した。Fr-M, D1, D2, T1, T2 について日立製 M-52 型 GC-MS で低電圧イオン化法 (LV：10eV) の質量分析を行った。GC 部には SE-52 FS-WCOT カラム 50m を用い、初温 100°C から 240°C まで 3°C/min. で昇温させ、繰り返し掃引で質量スペクトルを得た。得られた全スペクトルデータは MS 専用の日立 002B 及び M003 型電算機、これとオンラインで接続したパーソナルコンピュータで処理して、最終的に Z 数分子イオンスペクトルとして整理した。

2.3 モデル化合物の脱水素反応

ヒドロ芳香族モデル化合物として、テトラリン、1, 2, 3, 4, 9, 10, 4a, 9a オクタヒドロアントラセン (6 員環ナフテン)、アセナフテン、フルオレン (5 員環ナフテン) を混合比1:0.22:0.26:0.24の割合で調製して、モデル化合物とした。脱水素触媒は Pd-CaCO₃ (Aldrich 社) である。

モデル化合物とほぼ同量の触媒を内容積20ml のオートクレーブに充填し、窒素で置換、常圧とした。反応温度を350°C, 370°C, 390°C, 410°Cの各々で4時間反応させた。反応内容物をクロロホルムで抽出し、濾過、溶剤を留去させた後、GC-MS 分析を行った。

2.4 各化合物クラスの脱水素反応

HPLC 分別フラクションの Fr-M, D1, D2 の20-950mg とほぼ同量の Pd-CaCO₃ 触媒を加えて、モデル化合物の場合と同様な操作で脱水素反応を行った。但し反応温度は410°Cである。反応内容物は同様な処理によって生成物を得、GC-MS 分析を行った。更に、必要に応じて脱水素反応を繰り返した。

3. 結果と考察

3.1 化合物タイプの分布

HPLC-LV MS による構造解析法は芳香環及びこれにナフテン環の付いたヒドロ芳香環を表す「化合物タイプ」の解析であり、Z 数によって与えられる。この Z 数は分子の示性式 C_nH_{2n-Z} によって表せられる値で水素の不足数に相当する。分子量とは Mw=14n+Z の関係がある。また、芳香族炭素数 Ca, 芳香環とナフテン環を合わせた全環数 R と Z=2-(Ca+2R) で表される。

アミンカラムの HPLC によって、芳香環数毎の Fr-P (Ca=0), Fr-M (Ca=6), Fr-D1 (Ca=10), Fr-D2 (Ca=12), Fr-T (Ca>14) の各化合物クラスフラクションに分別されるので、Z 数の最大が限定される。更に上式の二つを満足させる真の Z 数が定まり、化合物タイプが決定できる¹²⁾。

HPLC による化合物クラスフラクションの収率は、Fr-P: 3.5, M: 3.5, D1: 19.7, D2: 7.3, T: 28.4, PP: 21.3 wt%である。図1は SRC-II 各化合物クラスについて、HPLC-LV MS による化合物タイプの分布である。各化合物クラス毎の芳香族環化合物 (ベンゼン類 (Fr-M, Z=-6), ナフタレン類 (Fr-D1, Z=-12), フェナントレン類 (Fr-T1, Z=-18), ピレン類 (Fr-T2, Z=-22)) の含有割合は、環数が多くなる程大きくなる傾向がある。言い換えれば芳香環数の少ない程その芳香環に付くナフテン環数の分布が広くなり、ヒドロ芳香族化合物の含有割合も大きくなる傾向が認められる。

3.2 ヒドロ芳香族モデル化合物の脱水素反応

図2はヒドロ芳香族モデル化合物及び反応温度410°Cにおける脱水素生成物の Z 数分子イオンスペクトルである。これよりヒドロ芳香族化合物の脱水素による化合物タイプの変化、並びに変化量が解析できる。図3は各反応温度における生成物分布の変化である。(M-I) の反応は350°Cでテトラリン (M-1) の42% (モル数) がナフタレン (M-2) に変化するが、410°Cでも最大60%で大きく変わらない。反応 (M-II) のオクタヒドロ体 (M-3) よりテトラヒドロ体 (M-4) への脱水素は350°Cで顕著に進行するが、更にアントラセン (M-5) への脱水素は390°C以上でなければ進行しない。9,10ジヒドロ体 (M-6) 経由の反応は僅かに起こる。これに対して、5員環ナフテンのアセナフテン (M-7), フルオレン (M-8) は反応しない。

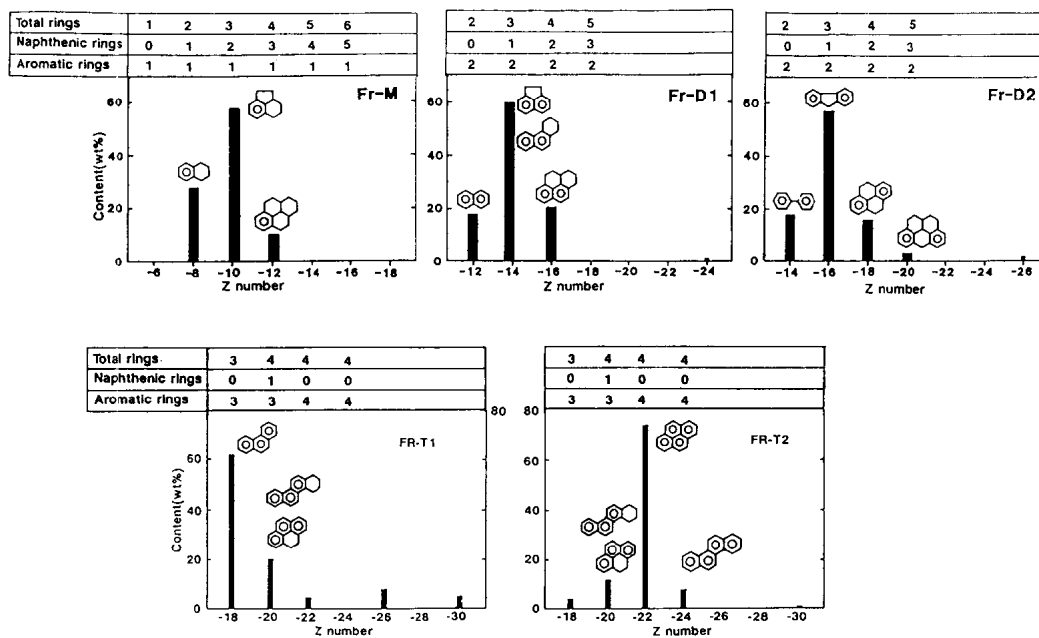


図1 各化合物クラス中の化合物タイプの分布

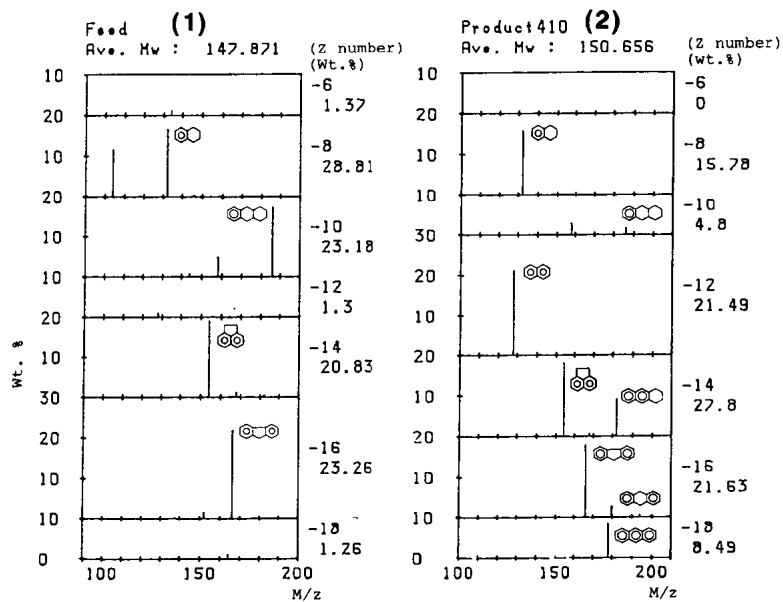


図2 ヒドロ芳香族モデル化合物(1)及びこの脱水素反応生成物(2)のZ数分子イオンスペクトル